Available online at www.sciencedirect.com

ScienceDirect

journal homepage: www.elsevier.com/locate/he

Evaluation of carbon supported platinum–ruthenium nanoparticles for ammonia electro-oxidation: Combined fuel cell and electrochemical approach

Júlio César M. Silva [a,b], *Spyridon Ntais* [a], *Érico Teixeira-Neto* [c], *Estevam V. Spinacé* [b], *Xiaoyu Cui* [d], *Almir O. Neto* [b], *Elena A. Baranova* [a,*]

[a] *Department of Chemical & Biological Engineering, Centre for Catalysis Research and Innovation (CCRI), University of Ottawa, 161 Louis-Pasteur, Ottawa, ON, K1N 6N5, Canada*

[b] *Instituto de Pesquisas Energéticas e Nucleares, IPEN/CNEN-SP, Av. Prof. Lineu Prestes, 2242 Cidade Universitária, CEP 05508-900, São Paulo, SP, Brazil*

[c] *Brazilian Nanotechnology National Laboratory, Brazilian Center for Research in Energy and Materials, Rua Giuseppe Máximo Scolfaro, 10.000, Campinas, SP, 13085-903, Brazil*

[d] *Canadian Light Source, Saskatoon, SK, S7N 2V3, Canada*

ARTICLE INFO

Article history:
Received 13 May 2016
Received in revised form
21 August 2016
Accepted 20 September 2016
Available online 24 November 2016

Keywords:
Ammonia electro-oxidation
PtRu/C nanoparticles
Electrolysis
Direct ammonia fuel cell

ABSTRACT

Ammonia electro-oxidation reaction (AmER) was investigated by using conventional electrochemical experiments, direct ammonia fuel cell (DAFC) and galvanostatic electrolysis experiments. The working electrode/anodes were composed of carbon supported PtRu/C nanoparticles (NPs) with atomic Pt:Ru ratios of 100:0, 90:10, 70:30 and 50:50. The resulting nanoparticles ranged between 5.1 and 7.3 nm in size depending on the Ru content and were analyzed by XRD, TEM and synchrotron radiation photoelectron Spectroscopy (SRPES). Alloying Pt with Ru shifted AmER to the lower onset potentials compared to Pt/C. Among nanostructured PtRu/C electrocatalysts, the $Pt_{90}Ru_{10}$ composition showed the best activity and stability in the conventional electrochemical (cyclic voltammetry and chronoamperometry) experiments, DAFC and 8 h galvanostatic electrolysis. The concentration of nitrite and nitrate was doubled using PtRu/C 90:10 compared to Pt/C, because of excess of OH_{ads} species formed on Ru. The results show that the addition of small amount of Ru to Pt NPs improves the AmER due to additional formation of OH_{ads} that promote the reaction on alloyed PtRu nanoparticles.

* *Corresponding author*. Fax: +1 6135625172.
E-mail address: elena.baranova@uottawa.ca (E.A. Baranova).

http://dx.doi.org/10.1016/j.ijhydene.2016.09.135

Introduction

The ammonia electro-oxidation reaction (AmER) has been extensively studied in the recently years from the different point of view, such as environmental applications, e.g., wastewater treatment and ammonia sensors and for energy generation in Direct Ammonia Fuel Cells (DAFCs) [1–9]. DAFC offers an important alternative to the current energy generation systems as clean and carbon-free fuel for efficient power source [4,10,11]. Ammonia has low production cost, is easy to handle and to transport [2,11], furthermore, the theoretical charge for ammonia oxidation to N_2 is 4.75 Ah g^{-1} that is very close to theoretical charge of methanol, 5.02 Ah g^{-1}, in its oxidation to CO_2 [2]. Moreover, liquid ammonia has 70% more hydrogen content and 50% higher specific energy density than liquid hydrogen per unit volume and is a carbon-free chemical energy carrier [12].

In this context different electrocatalysts have been evaluated for ammonia electro-oxidation in alkaline media [2–5,11–22]. Platinum is the most active catalyst for this process, however it suffers from deactivation by N_{ads} poisoning intermediate. The energy of N_{ads} on the catalyst surface is too high (−394 kJ mol^{-1} [13]), to enable the N_2 formation [23], as a consequence these strongly adsorbed intermediates block surface active sites and prevent continuous oxidation of ammonia on deactivated Pt surfaces. According to the literature, the degree of N_{ads} coverage on Pt surface increases with anodic potential and reaches the highest value at the peak current density of ammonia electro-oxidation in voltammetry experiments [14,15].

In order to overcome the deactivation of platinum by poisoning reaction intermediates and to increase the current density of AmER, Pt-binary electrocatalysts have been reported in the literature, such as PtIr [2,5,12,15,17], PtPd, $PtSnO_x$ [2,17], PtRh [2,4,5], PtNi [15] and PtRu [2,11,15]. It is well known that different factors, e.g., nanoparticle synthesis method, particle size, particle size distribution, surface and bulk structure, catalyst support, etc. play a role in electrocatalysis. In addition to these factors, the atomic ratio of Pt to the second metal influences AmER and the optimum performance varies depending on the second metal.

Among the reported bi-metallic catalysts, PtRu showed superior catalytic activity and stability towards AmER compared to monometallic Pt. For instance, Endo et al. [15] studied monometallic Pt and Ru and bi-metallic $Pt_{80}Ru_{20}$, and $Pt_{60}Ru_{40}$ catalysts prepared on carbon glass using thermal decomposition method. The authors showed that $Pt_{80}Ru_{20}$ had the highest current densities compared to other compositions. For $Pt_{80}Ru_{20}$, the onset potential was shifted by 100 mV to lower potential if compared to Pt, showing a synergetic effect between Pt and Ru. In the work by Vidal-Iglesias et al. [2], authors studied Pt_xRu_{1-x} (x = 100, 80, 50 and 20) unsupported nanoparticles synthesized using sodium borohydride in water/oil microemulsion method. They demonstrated using CV and CA experiments that the onset potential of AmER shifted about 100 mV to lower potential using $Pt_{80}Ru_{20}$ unsupported nanoparticles compared to Pt. In their study, $Pt_{50}Ru_{50}$ showed very low catalytic activity and $Pt_{20}Ru_{80}$ showed no activity at all [2].

Thus in both studies [2,15], the unsupported $Pt_{80}Ru_{20}$ combination showed the optimum performance, however the practical fuel cell catalysts are often composed of nanoparticles dispersed on high surface area support, e.g., carbon black. Therefore, in the present work PtRu/C electrocatalysts with different Pt:Ru atomic ratios: 100:0, 90:10, 70:30 and 50:50 were synthesized using facile and easy to scale-up borohydride reduction method and applied for AmER. For the first time, PtRu catalysts were tested in the direct ammonia fuel cell (DAFC) experiments in combination with detailed oxidation product evaluation during 8-h galvanostatic electrolysis.

Experimental

PtRu/C electrocatalysts (20 wt% of metals loading) with different Pt:Ru atomic ratios: 100:0, 90:10, 70:30, 50:50 were prepared by the sodium borohydride reduction process [10,24] using $H_2PtCl_6{\cdot}6H_2O$ (Sigma–Aldrich) and Ruthenium(III) chloride (Sigma–Aldrich), as metal sources. In this process Vulcan XC72 was first dispersed in an isopropyl alcohol/water solution (50/50, v/v). The mixture was homogenized under stirring and then the metal salts were added and put on an ultrasonic bath for 5 min. After that, a solution of $NaBH_4$ in 0.1 mol L^{-1} KOH was added in one portion under stirring at room temperature and the resulting solution was maintained under stirring for 15 min more. After this, the final mixture was filtered and the solids extensively washed with deionized water (18 MΩ) and then dried at 70 °C for 2 h.

The electrocatalysts were characterized by X-ray diffraction (XRD) using a Rigaku diffractometer model Miniflex II equipped with CuKα radiation source (0.15406 nm). The X-ray diffraction patterns were recorded between 20 and 90° 2θ with a step size of 0.05° and a scan time of 2 s per step. Transmission electron microscopy (TEM) images were carried out using a JEOL JEM2100F instrument and the atomic ratios of Pt and Ru in the synthesized materials were measured by energy dispersive spectroscopy (EDS) by using a JEOL − JSM6010 LA equipment. Synchrotron radiation photoelectron spectroscopy measurements (SRPES) were performed at the Variable Line Spacing Plane Grating Monochromator (PGM) beamline at the Canadian Light Source (CLS). The beamline is optimized for flux and brightness in the energy range of 5–200 eV. All spectra were recorded using the Scienta SES100 analyzer with a total energy resolution of 40 meV at room temperature with a system vacuum of 10^{-10} mbar.

Electrochemical measurements were carried out at room temperature using a potentiostat PARSTAT 2263 (Princeton Applied Research), using a three-electrode electrochemical cell made of teflon. A platinum electrode and a Hg/HgO were used as the counter and reference electrodes, respectively. Glassy carbon (GC) electrodes (0.166 cm^2) were used to deposit electrocatalysts. Before each experiment, the GC support was

polished with alumina suspension (1 μm) and washed in deionized water. Ultrapure deionized water obtained from a Milli-Q system (Millipore®) was used in all experimental procedures.

The catalyst "ink" was prepared by dispersing 6 mg of the electrocatalyst powder in 1 mL water, 100 μL isopropanol, and 100 μL of 5% Nafion® solution. The "ink" was sonicated in an ultrasonic bath for 30 min. Subsequently, aliquots of 8 μL of the dispersion was deposited onto the GC surface and air dried at 60 °C.

Cyclic voltammograms in 1 M KOH and 1 M (KOH + NH_4OH) were carried out at a scan rate of 20 mV s^{-1} between −0.85 and 0.2 V vs. Hg/HgO. The electrocatalysts were cycled for 10 consecutive cycles resulting in the stable and reproducible shape of the voltammogram in ammonia free solutions and for 3 consecutive cycles in ammonia containing solutions. The third scan of CVs is reported unless otherwise stated. Chronoamperometric experiments were carried out for 2 h at −0.30 V and −0.25 V *vs.* Hg/HgO.

The catalyst electrochemical active surface area (ECSA) was determined by stripping experiments of CO monolayers, integrating the CO_{ad} stripping charges, assuming the factor of 420 μC cm^{-2} [25]. In this procedure the mixture of CO (1% in He, Linde) was bubbled through 1 M KOH solution for 20 min while the potential was held at −0.6 V, then pure N_2 (99.99%, Linde) was bubbled for 20 min to remove the dissolved CO from the solution. The CO stripping voltammograms were then recorded at a scan rate of 20 mV s^{-1}. The estimated ECSA values for Pt/C, $Pt_{90}Ru_{10}$/C, $Pt_{70}Ru_{30}$/C, $Pt_{50}Ru_{50}$/C were 1.00, 0.87, 0.72 and 0.42 cm^2, respectively. The ammonia current from electrochemical experiments was normalized per ECSA unless otherwise stated.

DAFCs experiments were conducted using 1 M (NH_4OH + KOH) as already described in details elsewhere [3,4,10,18]. In these experiments, a single cell set at 50 °C with an electrode area of 5 cm^2 was employed. The electrocatalyst was painted over carbon cloth in the form of a homogeneous dispersion prepared using Nafion solution (5 wt%, Aldrich). The temperature of the oxygen humidifier was maintained at 85 °C. The mass of catalyst at the anode and the cathode was 1 and 2 mg cm^{-2}, respectively. For all experiments, a commercial Pt/C (BASF) with 20 wt% of metals loading was used as cathode. A Nafion® 117 membrane previously exposed to 6 mol L^{-1} KOH for 24 h [3,4,10,26] was used for fuel cell experiments.

The bulk galvanostatic electrolysis of 0.2 M of NH_4OH in 1 M KOH was carried out on Pt/C and $Pt_{90}Ru_{10}$/C electrocatalysts at 25 mA cm^{-2} for 8 h under vigorous stirring and at room temperature. The working electrode was prepared by depositing and draying overnight 80 μL of the catalysts ink onto a 1.27 cm^{-2} carbon fiber paper (SpectraCarb 250-A, Fuel Cell Store). A large surface stainless steel spring of grade 304 served as a counter electrode and was kept in a separate compartment. Analysis of the by-products of ammonia electro-oxidation was done by collecting 0.5 mL samples every 1 h. Ammonia was determined according to the procedure stipulated in Standard Methods 1985. The determination of nitrite and nitrate concentrations was performed using Hach analytical kit [12]. Each sample was analyzed three times with a reproducibility of ±0.1 mg N L^{-1}.

Results and discussion

Physicochemical characterizations of Pt/C and PtRu/C catalysts

Fig. 1 shows the X-ray diffraction patterns of the carbon supported Pt and PtRu electrocatalysts. The broad peak at around 25 °2θ that is assigned to the (022) reflection of graphite in Vulcan XC-72 carbon [17,18]. The peaks at around 40, 46, 67, 81 °2θ are attributed to the (111), (200), (220) and (311) face centered cubic (fcc) reflections typical for bulk and nanostructured Pt [4,18]. The diffraction peaks in the PtRu catalysts are shifted to higher 2θ values with respect to the same reflections in Pt/C (Table 1), suggesting the platinum ruthenium alloy formation [27,28], however because the main (111) and (200) Pt reflections overlap with graphite reflection (101) at 45 °2θ in carbon Vulcan XC-72, the crystallite size analysis was done using (220) reflection and Scherrer equation [17,29].

Table 1 shows that the crystallite sizes of $Pt_{70}Ru_{30}$/C and $Pt_{50}Ru_{50}$/C were lower than that of Pt/C and $Pt_{90}Ru_{10}$/C materials. The composition of the PtRu/C electrocatalysts obtained by the EDS analysis is presented in Table 1. The experimental atomic composition obtained by EDS analysis are very close to the nominal ones, showing that sodium borohydride is effective for the simultaneous reduction of platinum and ruthenium ions.

The TEM micrographs and histogram of the particles sizes are shown in Fig. 2. As can be seen in Fig. 2a, Pt nanoparticles show non-uniform dispersion on carbon support, i.e., in addition to single particles some particle agglomeration (up to 33 nm in size) is also present. The histogram of Pt/C shows that most of nanoparticles are smaller than 12 nm with presence of large agglomerates. PtRu nanoparticles are relatively well dispersed on the support (Fig. 2b) although some particle aggregation was also observed. Histogram of $Pt_{90}Ru_{10}$/C confirmed that the average particle size is smaller than 10 nm and the heterogeneity in terms of particles size is smaller than for Pt/C. As can be observed from TEM images of $Pt_{70}Ru_{30}$/C (Fig. 2c) and $Pt_{50}Ru_{50}$/C (Fig. 2d) catalysts, the

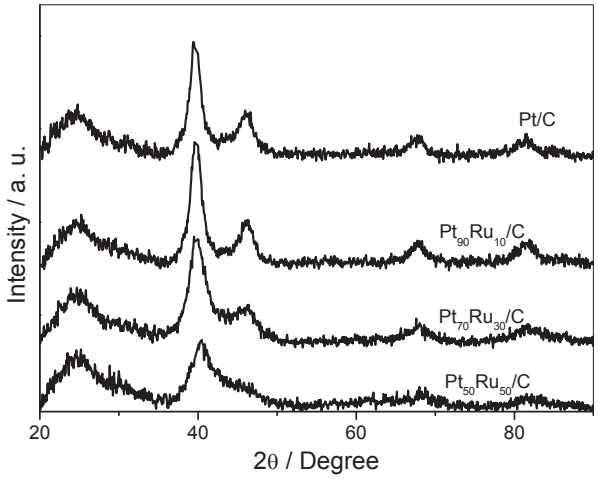

Fig. 1 – X-ray diffraction patterns of the Pt/C and PtRu/C electrocatalysts.

Table 1 – Characteristics of carbon-supported Pt and PtRu catalysts.

Electrocatalyst nominal atomic composition (%)	Atomic composition (%) from EDS	Crystallite size (nm) from (220) peak	2 θ_{max} of (111) (°)	Average particles sizes (nm) from TEM
Pt/C	–	4.3	39.64	7.3
$Pt_{90}Ru_{10}/C$	90:10	4.5	39.79	5.7
$Pt_{70}Ru_{30}/C$	69:31	3.6	39.85	5.2
$Pt_{50}Ru_{50}/C$	51:49	3.3	40.37	5.1

nanoparticles size is similar for both materials and both show good dispersion on the carbon support. The nanoparticle mean diameters are summarized in Table 1. Form the TEM micrographs it is possible to conclude that the nanoparticles become smaller and better dispersed on the carbon support as the ruthenium content in Pt increases.

The observed heterogeneity in Pt nanoparticles sizes with the average size below 10 nm is characteristic of the sodium borohydride synthesis method [3,10,30,31].

Synchrotron radiation photoelectron spectroscopy studies were carried out for all catalysts synthesized in the present work. Fig. 3 shows the Pt4f peaks. The exact positions, full width at half maximum (FWHM) and the percentage ration of each component of Pt4f peak are summarized in Table 2. The analysis of the recorded peaks revealed the existence of platinum atoms in two different states. More specifically, the component at lower BE is attributed to metallic Pt representing around 85% of the peak area, while the component at higher BE, is due to Pt^{2+} [32].

As can be seen, the peak positions are similar for the Pt/C and the $Pt_{90}Ru_{10}/C$, however the Pt4f peak shifts towards higher BEs as the Ru content increases. More specifically, a shift of around 0.08 eV is observed for the Pt^0 component in the case of the $Pt_{70}Ru_{30}/C$ compared to the position of the corresponding component in the case of the Pt/C. The observed shift is even more pronounced for $Pt_{50}Ru_{50}/C$ and more specifically the Pt^0 component is detected at 71.60 eV, which is 0.24 eV towards higher BEs. Our results and the positive shifts of the Pt4f SRPES peak are in agreement with previous studies [33–35], where nanosized Pt–Ru systems have been studied in details using both traditional and synchrotron radiation induced photoelectron spectroscopy, as well as theoretical calculations. These studies [33–35] have shown that the Pt4f peak shows significant shift towards higher binding energy for alloyed PtRu catalysts compared to monometallic Pt or platinum foil, whereas the reported shifts of the corresponding Ru3d peaks were significantly lower [33–35]. Furthermore, the Ru4p state was detected around 44 eV and exhibited considerably low flux and signal-noise-ratio under our experimental conditions and even after prolonged scanning the peak was ill defined, thus not allowing us to obtain more detailed information concerning the oxidation state of ruthenium atoms in PtRu/C NPs. We also need to point out that the used synchrotron assisted photoelectron spectroscopy technique is very surface sensitive and can only detect the electrons escaped from few Angstroms surface region. This may indicate that there are less Ru atoms at the surface than in the bulk, compared with relative large-region-ordered Pt atoms.

The observed shift of the Pt4f peak is a strong evidence that Pt and Ru are alloyed in agreement with XRD data. The fact that the work function of Ru (~4.71 eV) is lower than that of Pt (~5.74 eV) [36], means that electrons should flow from the former to the latter metal, thus increasing the electron density around platinum atoms, causing the shift of the Pt4f towards lower BEs. However, the observed positive shift of the Pt4f peak can be explained by the re-hybridization of the d- and sp-band [37] and changes in the bond distances as the composition of the NPs change and the Ru content increases.

Cyclic voltammetry and chronoamperometry of Pt/C and PtRu/C catalysts

The cyclic voltammetry of Pt/C and PtRu/C electrocatalysts in 1 M KOH in the potential range of −0.85 V to 0.2 V are shown in Fig. 4. For Pt/C and $Pt_{90}Ru_{10}/C$, two peaks related to hydrogen adsorption/desorption process at about −0.63 V and −0.53 V are present on CVs [4,38]. The region from −0.20 to 0.2 V in the anodic scan is associated with the formation of Pt oxides [4,39]. In the reverse scan, Pt oxide reduction takes place at around − 0.18 V on Pt/C [4,40], whereas the cathodic peak shifts to lower potential values as Ru content in PtRu/C increases. As can be seen the shape of the CV of Pt/C and $Pt_{90}Ru_{10}/C$ are similar, because of the small amount of Ru in the $Pt_{90}Ru_{10}/C$ composition. As the Ru content increases the charging currents increases and the Pt and Ru oxide reduction peak shifts to lower potentials: −0.32 and −0.38 V for $Pt_{70}Ru_{30}/C$ and $Pt_{50}Ru_{50}/C$, respectively [27]. For $Pt_{70}Ru_{30}/C$ and $Pt_{50}Ru_{50}/C$, the two peaks related to hydrogen adsorption/desorption process were suppressed due to the high amount of ruthenium content, similar behavior was also observed in the literature [38,41]. The obtained current values were normalized by the ECSA, which was estimated from the CO stripping experiments. The estimated ECSA values for Pt/C, $Pt_{90}Ru_{10}/C$, $Pt_{70}Ru_{30}/C$, $Pt_{50}Ru_{50}/C$ were 1.00, 0.87, 0.72 and 0.42 cm^2, respectively. As can be seen the ECSA decreases as the amount of Pt decreases, this behavior was also observed earlier for the materials prepared by the same method [42]. This is in agreement with the bifunctional mechanism in which the CO is mostly adsorbed on the Pt atoms. The role of Ru is to provide oxygenated species (Ru-OH) to promote the CO electro-oxidation [43,44]. Thus, the CO stripping charge would represent the total amount of Pt atoms at the surface of the materials.

Fig. 5 shows the CVs of Pt/C and PtRu/C (90:10, 70:30, 50:50 at %) electrocatalysts in 1 M (KOH + NH_4OH). The onset potential for ammonia electro-oxidation shifts to lower potential as the ruthenium content in the materials increases. However, at high amount of ruthenium ($Pt_{70}Ru_{30}/C$ and $Pt_{50}Ru_{50}/C$) the peak current density for ammonia electro-oxidation decreases significantly if compared to Pt/C and $Pt_{90}Ru_{10}/C$. It has

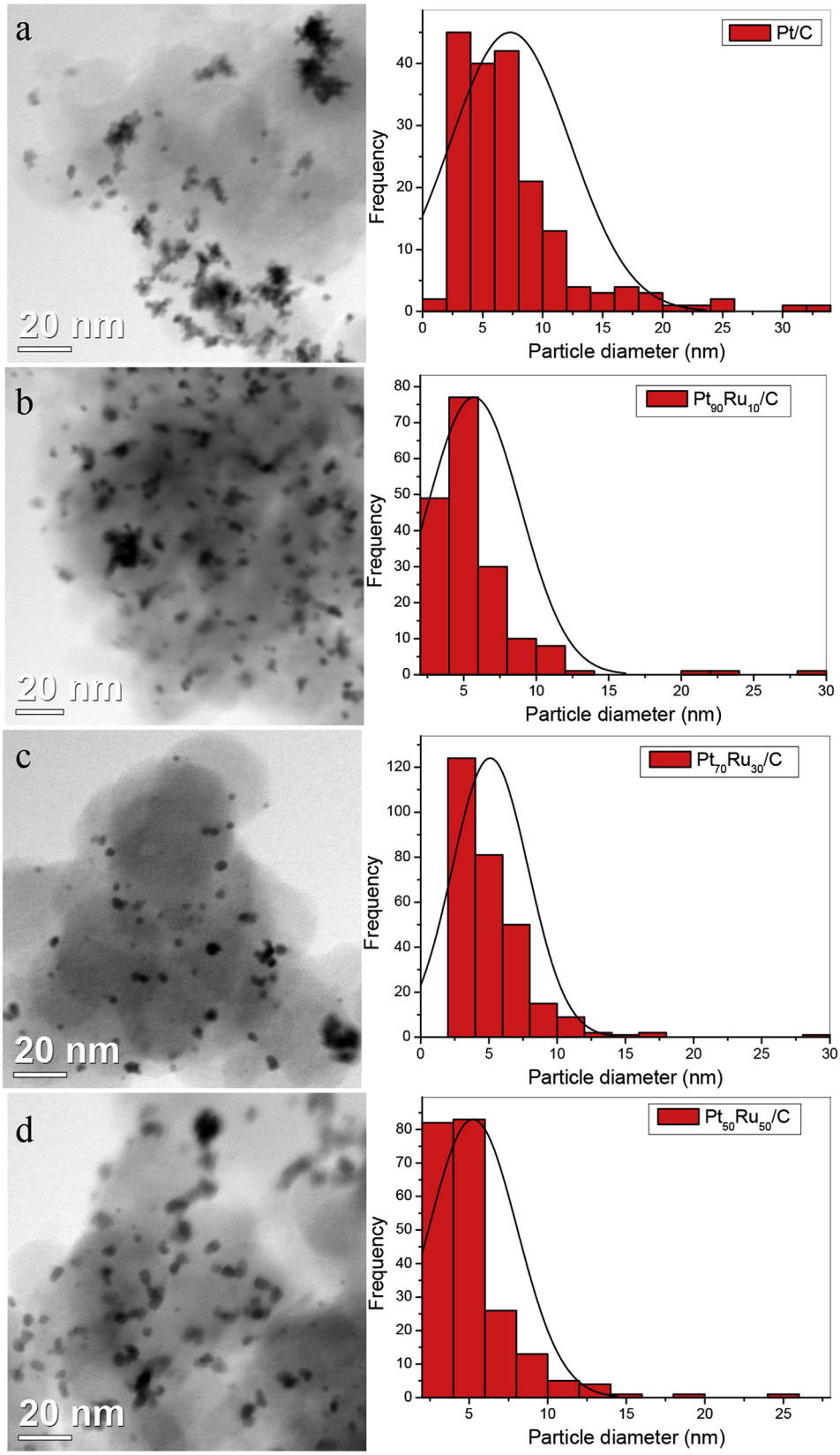

Fig. 2 – The TEM micrographs (left) and corresponding histograms (right) of Pt/C (a), $Pt_{90}Ru_{10}$/C (b), $Pt_{70}Ru_{30}$/C (c) and $Pt_{50}Ru_{50}$/C (d).

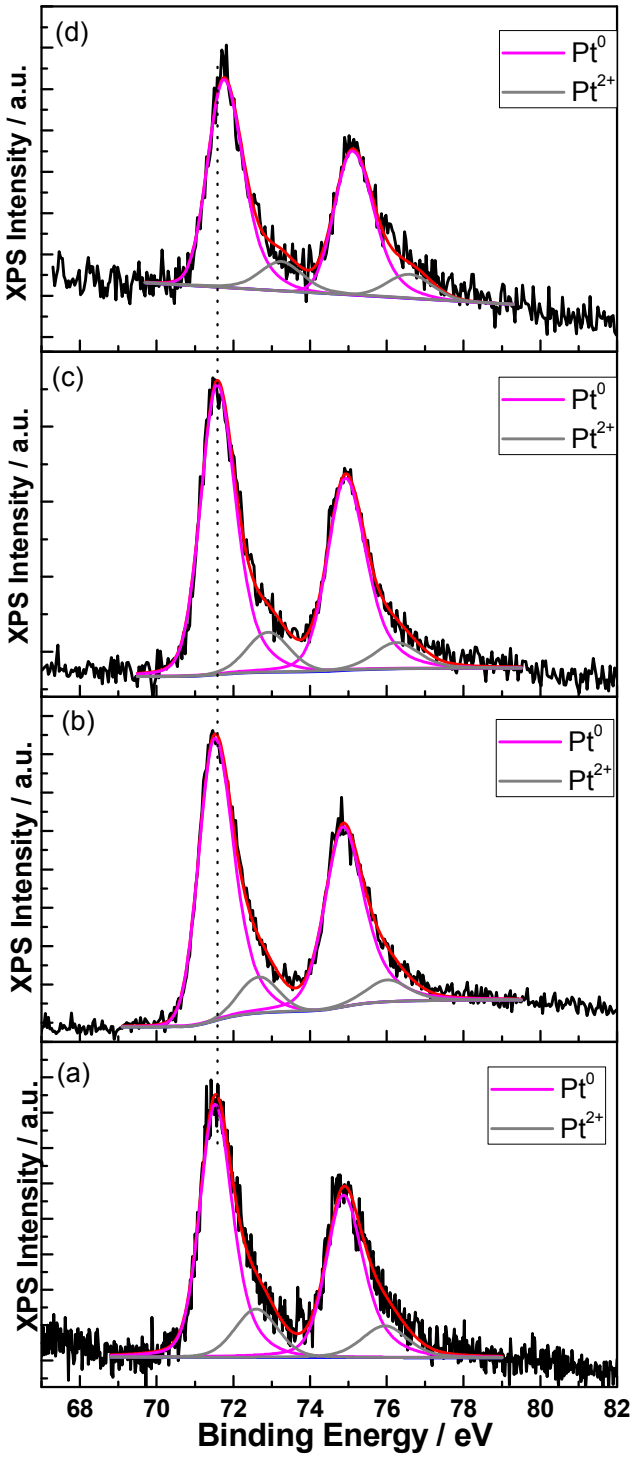

Fig. 3 – Pt4f SRPES peaks for (a) Pt/C, (b) $Pt_{90}Ru_{10}$/C, (c) $Pt_{70}Ru_{30}$/C and (d) $Pt_{50}Ru_{50}$/C.

already been reported in the literature that atomic compositions of ruthenium higher than 20% in the PtRu electrocatalyst causes a decrease in the peak current density for ammonia electro-oxidation process [2,15]. Furthermore, the highest peak current density was obtained using $Pt_{90}Ru_{10}$/C showing that small amount of Ru improves the catalytic activity of platinum towards ammonia electro-oxidation reaction. The enhanced catalytic activity of $Pt_{90}Ru_{10}$/C may be related to the fact that Ru is able to dehydrogenate ammonia at lower potential than Pt [13], because ammonia dehydrogenation is an important step in the electro-oxidation process. However, as Ru content increases the activity decreases indicating that Ru-rich surfaces are not suitable for ammonia oxidation probably due to the high amount of N_{ads} on the Ru surface, because the theoretically calculated adsorption energy of N on Ru is higher than on Pt [13].

Table 2 – Summary of SRPES analysis: Pt4f peak position, full width at half maximum (FWHM) and the percentage ratio of Pt^0 and Pt^{2+}.

Electrocatalyst	Peak position (eV)	FWHM (eV)	At.%	Assignment
Pt/C	71.36	0.94	82.2	Pt^0
	72.45	1.27	17.8	Pt^{2+}
$Pt_{90}Ru_{10}$/C	71.35	0.95	87.8	Pt^0
	72.46	1.3	12.2	Pt^{2+}
$Pt_{70}Ru_{30}$/C	71.44	0.99	87.1	Pt^0
	72.75	1.3	12.9	Pt^{2+}
$Pt_{50}Ru_{50}$/C	71.60	0.92	86.1	Pt^0
	72.68	1.28	13.9	Pt^{2+}

Fig. 6 shows the chronoamperometric curves in 1 M (KOH + NH_4OH) on Pt/C, $Pt_{90}Ru_{10}$/C and $Pt_{70}Ru_{30}$/C nanoparticles at −0.25 V during 2 h. As can be seen, the current density decreases significantly within the first hour but becomes less pronounced after 1.5 h. The continues current decline is due to the surface poisoning by the inactive intermediates, e.g., N_{ads} as was also reported in the literature for various Pt-based catalysts [3,4,17]. The current density for ammonia electro-oxidation after 2 h experiment on $Pt_{90}Ru_{10}$/C was about 2.5 times higher than that on Pt/C and $Pt_{70}Ru_{30}$/C, while $Pt_{50}Ru_{50}$/C showed negligible current density in CA measurements (not shown here). Thus, addition of 10 at.% of Ru improved Pt activity and stability against deactivation by providing oxygenated surface species

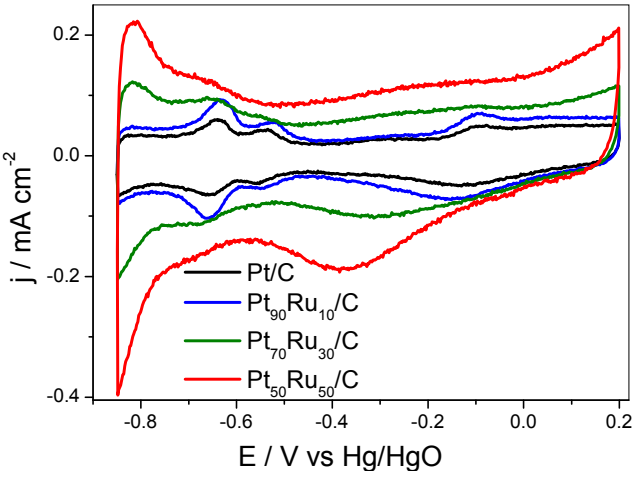

Fig. 4 – Cyclic voltammograms for Pt/C, $Pt_{90}Ru_{10}$/C, $Pt_{70}Ru_{30}$/C and $Pt_{50}Ru_{50}$/C electrocatalysts in 1 M KOH at $\nu = 20$ mV s^{-1}.

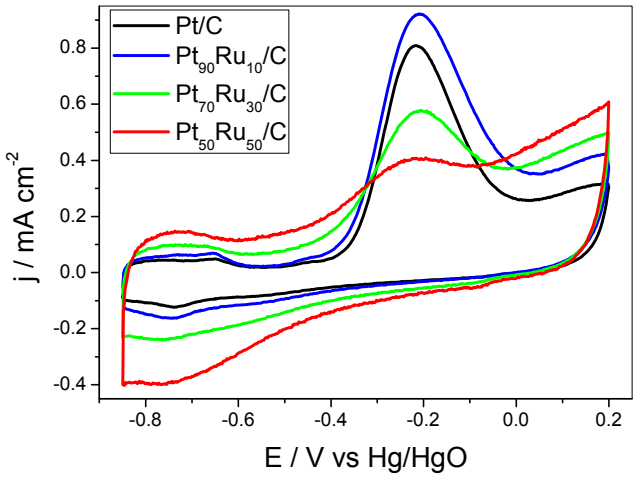

Fig. 5 – Cyclic voltammograms for Pt/C, $Pt_{90}Ru_{10}$/C, $Pt_{70}Ru_{30}$/C and $Pt_{50}Ru_{50}$/C electrocatalysts in 1 M (KOH + NH_4OH). Scan rate of 20 mV s^{-1}.

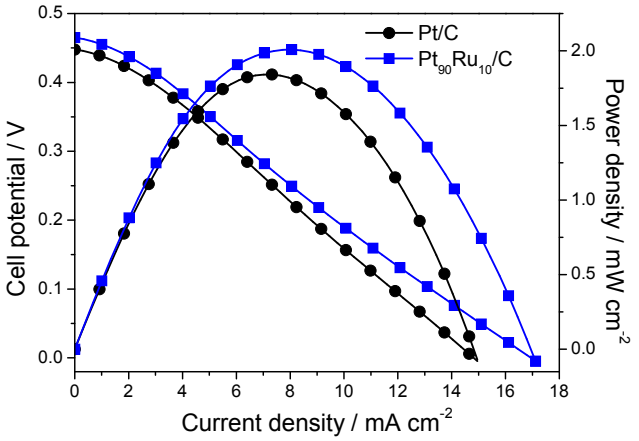

Fig. 7 – Polarization and power density curves of a 5 cm^2 DAFC at 50 °C using 1 M (NH_4OH + KOH).

without compromising the adsorption of ammonia on Pt or PtRu neighboring sites. It is well illustrated in the literature that Ru surfaces form OH_{ads} at considerably lower potentials than platinum [43,45,46]. Moreover, the electronic affect generated in PtRu alloys [47–50] helps dehydrogenation of ammonia at lower potentials thus contributing towards the increase of the catalytic activity of $Pt_{90}Ru_{10}$ for AmER [4,10,12]. The low catalytic activity of $Pt_{50}Ru_{50}$/C is in agreement with the earlier report [2].

Direct ammonia fuel cell

The best performing $Pt_{90}Ru_{10}$/C electrocatalyst was tested as an anode in the DAFC experiments and compared to Pt/C. Fig. 7 shows the cell voltage and power density as a function of the current density obtained for 1 M (NH_4OH + KOH) as fuel at 50 °C using commercial Pt/C (BASF) as cathode. The open circuit voltage (OCV) was 0.47 V and 0.45 V using $Pt_{90}Ru_{10}$/C and Pt/C as an anode, respectively. Suzuki at al. [11] also reported the higher OCV using PtRu/C (0.54 V) than Pt/C (0.37 V), however their experiments were done using NH_3 gas and electrocatalysts loading of ~45 wt% compared 20 wt% in the present study. The higher OCV obtained using $Pt_{90}Ru_{10}$/C confirms its superior catalytic activity for AmER [10,11]. The power density curves reveal that the maximum power density using $Pt_{90}Ru_{10}$/C was almost 10% higher than that obtained using Pt/C. It is also possible to observe from Fig. 5 that the current density was about 15% higher for $Pt_{90}Ru_{10}$/C than Pt/C. The OCV and the maximum power density obtained using Pt/C is in agreement with the previous publication [18]. Thus, $Pt_{90}Ru_{10}$/C showed the best fuel cell performance among all the catalysts synthesized in the present work in agreement with CV and CA experiments.

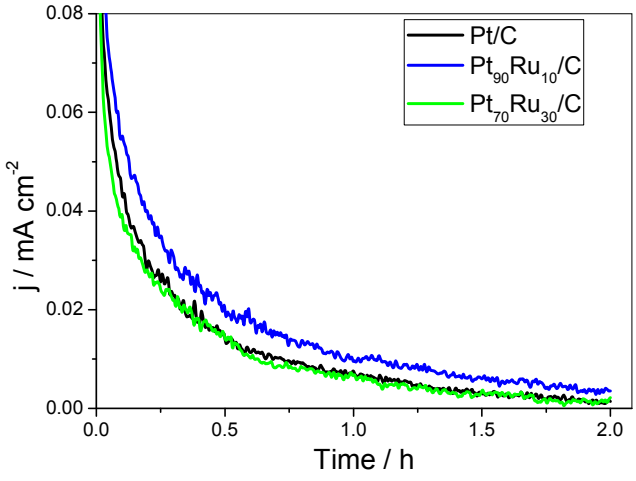

Fig. 6 – Chronoamperometric measurements at −0.25 V vs Hg/HgO for Pt/C, $Pt_{90}Ru_{10}$/C, $Pt_{70}Ru_{30}$/C and $Pt_{50}Ru_{50}$/C electrocatalysts in 1 M (KOH + NH_4OH).

Galvanostatic electrolysis

In order to evaluate the oxidation products over Pt/C and $Pt_{90}Ru_{10}$/C electrocatalysts, the 8 h galvanostatic electrolysis

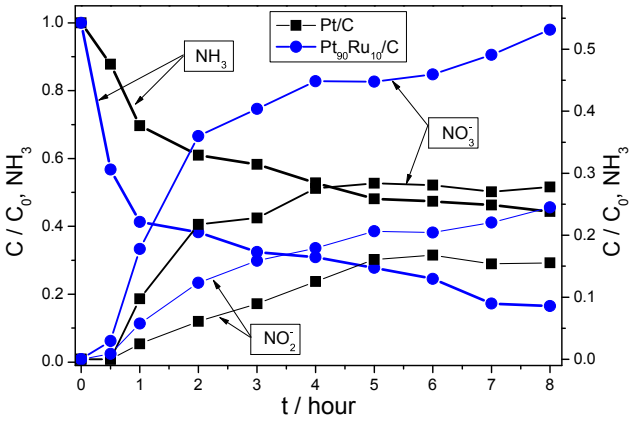

Fig. 8 – The normalized concentration profile of ammonia, nitrite and nitrite during electrolysis of ammonia under galvanostatic conditions on Pt/C and $Pt_{90}Ru_{10}$/C in 1 M KOH + 0.2 M NH_4OH, i = 25 mA cm^{-2}.

experiments in 0.2 M NH_4OH + 1 M KOH at 25 mA cm^{-2} were carried out. Fig. 8 shows the normalized concentration of ammonia, nitrite and nitrate as a function of time. The concentration of ammonia decreased with time using both materials, however, after 8 h, 84% of initial ammonia was degraded on $Pt_{90}Ru_{10}$/C and only 66% on Pt/C. The main products of ammonia oxidation were N_2, NO_3^- and NO_2^-. It has been reported that ammonia electro-oxidation on metal oxides results in predominant formation of oxygenated nitrogen species [13,17] and that ruthenium is not selective to oxidize ammonia to N_2 [13]. According to Gootzen at al. [14] oxygenated species are involved in the NO_2^- and NO_3^- formation during ammonia electro-oxidation. The concentration of nitrate and nitrite produced on $Pt_{90}Ru_{10}$/C were about twice as higher as on Pt/C, due to the excess of OH_{ads} species formed on Ru at lower potentials [43,45,46].

Conclusion

In the present work we demonstrated that addition of 10 at.% of Ru to Pt nanoparticles ($Pt_{90}Ru_{10}$/C) improved the catalytic activity of Pt towards ammonia electro-oxidation as shown by detailed electrochemical and fuel cell experiments. The XRD results showed formation of PtRu alloy for all bimetallic compositions. The SRPES analysis revealed that high amount of Pt is present in metallic phase and further confirmed the PtRu alloy formation. According to TEM micrographs, Pt/C and $Pt_{90}Ru_{10}$/C nanoparticles were more heterogeneously dispersed than $Pt_{70}Ru_{30}$/C and $Pt_{50}Ru_{50}$/C, however for all the materials, the average particle size was below 10 nm. Among all the materials, the $Pt_{90}Ru_{10}$/C showed the highest catalytic activity. The $Pt_{90}Ru_{10}$/C outperformed Pt/C as anode in DAFC experiments. Using $Pt_{90}Ru_{10}$/C the OCV was 20 mV higher than on Pt/C, also the maximum power density and current density were about 10% and 15% higher if compared to Pt/C.

The electrolysis results showed that initial ammonia concentration decreased by 84 and 66% after 8 h experiment using $Pt_{90}Ru_{10}$/C and Pt/C, respectively. Furthermore, the concentration of nitrite and nitrate were twice higher using PtRu/C 90:10 than using Pt/C, therefore confirming that Ru addition provides abundance of OH_{ads} species that play a key role in ammonia oxidation reaction.

Acknowledgements

The authors wish to thank FAPESP process numbers (2013/01577-0, 2014/09868-6) and CNPq for the financial support. Use of TEM facilities (JEOL JEM-2100F) of LNNano-CNPEM is greatly acknowledge. The help of Dr. Fares Al-Momani from the University of Qatar with the reaction product analysis is greatly acknowledged.

A portion of the research described in this paper was performed at the Canadian Light Source, which is funded by the Canada Foundation for Innovation, NSERC, the National Research Council Canada, the Canadian Institutes of Health Research, the Government of Saskatchewan, Western Economic Diversification Canada, and the University of Saskatchewan.

REFERENCES

[1] Bunce NJ, Bejan D. Mechanism of electrochemical oxidation of ammonia. Electrochim Acta 2011;56:8085–93.
[2] Vidal-Iglesias FJ, Solla-Gullón J, Montiel V, Feliu JM, Aldaz A. Screening of electrocatalysts for direct ammonia fuel cell: ammonia oxidation on PtMe (Me: Ir, Rh, Pd, Ru) and preferentially oriented Pt(100) nanoparticles. J Power Sources 2007;171:448–56.
[3] Assumpção MHMT, da Silva SG, De Souza RFB, Buzzo GS, Spinacé EV, Santos MC, et al. Investigation of PdIr/C electrocatalysts as anode on the performance of direct ammonia fuel cell. J Power Sources 2014;268:129–36.
[4] Assumpção MHMT, Piasentin RM, Hammer P, De Souza RFB, Buzzo GS, Santos MC, et al. Oxidation of ammonia using PtRh/C electrocatalysts: fuel cell and electrochemical evaluation. Appl Catal B Environ 2015;174–175:136–44.
[5] Boggs BK, Botte GG. Optimization of Pt–Ir on carbon fiber paper for the electro-oxidation of ammonia in alkaline media. Electrochim Acta 2010;55:5287–93.
[6] Metkemeijer R, Achard P. Proceedings of the Third Grove Fuel Cell Symposium The Science, Engineering and Practice of Fuel Cells Ammonia as a feedstock for a hydrogen fuel cell; reformer and fuel cell behaviour. J Power Sources 1994;49:271–82.
[7] Kapałka A, Fierro S, Frontistis Z, Katsaounis A, Neodo S, Frey O, et al. Electrochemical oxidation of ammonia (NH4+/NH_3) on thermally and electrochemically prepared IrO_2 electrodes. Electrochim Acta 2011;56:1361–5.
[8] Cairns EJ, Simons EL, Tevebaugh AD. Ammonia-oxygen fuel cell. Nature 1968;217:780–1.
[9] Kapałka A, Fierro S, Frontistis Z, Katsaounis A, Frey O, Koudelka M, et al. Electrochemical behaviour of ammonia () on electrochemically grown anodic iridium oxide film (AIROF) electrode. Electrochem Commun 2009;11:1590–2.
[10] Assumpção MHMT, da Silva SG, de Souza RFB, Buzzo GS, Spinacé EV, Neto AO, et al. Direct ammonia fuel cell performance using PtIr/C as anode electrocatalysts. Int J Hydrogen Energy 2014;39:5148–52.
[11] Suzuki S, Muroyama H, Matsui T, Eguchi K. Fundamental studies on direct ammonia fuel cell employing anion exchange membrane. J Power Sources 2012;208:257–62.
[12] Allagui A, Oudah M, Tuaev X, Ntais S, Almomani F, Baranova EA. Ammonia electro-oxidation on alloyed PtIr nanoparticles of well-defined size. Int J Hydrogen Energy 2013;38:2455–63.
[13] de Vooys ACA, Koper MTM, van Santen RA, van Veen JAR. The role of adsorbates in the electrochemical oxidation of ammonia on noble and transition metal electrodes. J Electroanal Chem 2001;506:127–37.
[14] Gootzen JFE, Wonders AH, Visscher W, van Santen RA, van Veen JAR. A DEMS and cyclic voltammetry study of NH_3 oxidation on platinized platinum. Electrochim Acta 1998;43:1851–61.
[15] Endo K, Nakamura K, Katayama Y, Miura T. Pt–Me (Me = Ir, Ru, Ni) binary alloys as an ammonia oxidation anode. Electrochim Acta 2004;49:2503–9.
[16] Allagui A, Sarfraz S, Baranova EA. NixPd1−x (x= 0.98, 0.93, and 0.58) nanostructured catalysts for ammonia

electrooxidation in alkaline media. Electrochim Acta 2013;110:253–9.
[17] Lomocso TL, Baranova EA. Electrochemical oxidation of ammonia on carbon-supported bi-metallic PtM (M = Ir, Pd, SnO_x) nanoparticles. Electrochim Acta 2011;56:8551–8.
[18] Silva JCM, da Silva SG, De Souza RFB, Buzzo GS, Spinacé EV, Neto AO, et al. PtAu/C electrocatalysts as anodes for direct ammonia fuel cell. Appl Catal A General 2015;490:133–8.
[19] Liu J, Zhong C, Yang Y, Wu YT, Jiang AK, Deng YD, et al. Electrochemical preparation and characterization of Pt particles on ITO substrate: morphological effect on ammonia oxidation. Int J Hydrogen Energy 2012;37:8981–7.
[20] Hung C-M. Electrochemical properties of PtPdRh alloy catalysts for ammonia electrocatalytic oxidation. Int J Hydrogen Energy 2012;37:13815–21.
[21] Yao K, Cheng YF. Fabrication by electrolytic deposition of Pt–Ni electrocatalyst for oxidation of ammonia in alkaline solution. Int J Hydrogen Energy 2008;33:6681–6.
[22] He S, Wu Z, Li S, Lee J-M. Ionic liquid-assisted synthesis of platinum nanocubes and their improved electrocatalytic activity for the ammonia oxidation reaction. Int J Hydrogen Energy 2016;41:1990–6.
[23] Gerischer H, Mauerer A. Untersuchungen Zur anodischen Oxidation von Ammoniak an Platin-Elektroden. J Electroanal Chem Interfacial Electrochem 1970;25:421–33.
[24] Neto AO, da Silva SG, Buzzo GS, de Souza RFB, Assumpção MHMT, Spinacé EV, et al. Ethanol electrooxidation on PdIr/C electrocatalysts in alkaline media: electrochemical and fuel cell studies. Ionics 2015;21:487–95.
[25] Jiang Q, Jiang L, Qi J, Wang S, Sun G. Experimental and density functional theory studies on PtPb/C bimetallic electrocatalysts for methanol electrooxidation reaction in alkaline media. Electrochim Acta 2011;56:6431–40.
[26] Hou H, Wang S, Jin W, Jiang Q, Sun L, Jiang L, et al. KOH modified Nafion112 membrane for high performance alkaline direct ethanol fuel cell. Int J Hydrogen Energy 2011;36:5104–9.
[27] Lizcano-Valbuena WH, Paganin VA, Gonzalez ER. Methanol electro-oxidation on gas diffusion electrodes prepared with Pt-Ru/C catalysts. Electrochim Acta 2002;47:3715–22.
[28] Baranova EA, Le Page Y, Ilin D, Bock C, MacDougall B, Mercier PHJ. Size and composition for 1–5nm Ø PtRu alloy nano-particles from Cu Kα X-ray patterns. J Alloys Compd 2009;471:387–94.
[29] Silva JCM, Anea B, De Souza RFB, Assumpcao MHMT, Calegaro ML, Neto AO, et al. Ethanol oxidation reaction on IrPtSn/C electrocatalysts with low Pt content. J Braz Chem Soc 2013;24:1553–60.
[30] Neto AO, da Silva SG, Buzzo GS, de Souza RFB, Assumpção MHMT, Spinacé EV, et al. Ethanol electrooxidation on PdIr/C electrocatalysts in alkaline media: electrochemical and fuel cell studies. Ionics 2014:1–9.
[31] da Silva SG, Silva JCM, Buzzo GS, De Souza RFB, Spinacé EV, Neto AO, et al. Electrochemical and fuel cell evaluation of PtAu/C electrocatalysts for ethanol electro-oxidation in alkaline media. Int J Hydrogen Energy 2014;39:10121–7.
[32] Isaifan RJ, Ntais S, Baranova EA. Particle size effect on catalytic activity of carbon-supported Pt nanoparticles for complete ethylene oxidation. Appl Catal A General 2013;464–465:87–94.
[33] Lewera A, Zhou WP, Hunger R, Jaegermann W, Wieckowski A, Yockel S, et al. Core-level binding energy shifts in Pt–Ru nanoparticles: a puzzle resolved. Chem Phys Lett 2007;447:39–43.
[34] Alayoglu S, Nilekar AU, Mavrikakis M, Eichhorn B. Ru-Pt core-shell nanoparticles for preferential oxidation of carbon monoxide in hydrogen. Nat Mater 2008;7:333–8.
[35] Chen T-Y, Liu Y-T, Nguyen HM, Fan L-J, Wu C-Y, Mark Luo T-J, et al. Ruthenium core-activated platinum monolayer shell high redox activity cathodic electrocatalysts for dye-sensitized solar cells. J Mater Chem A 2013;1:5660–9.
[36] Hölzl J, Schulte F, Wagner H. Solid surface physics. Berlin: Springer-Verlag; 1979. p. 85. Print. Springer Tracts in Modern Physics.
[37] Weinert M, Watson RE. Core-level shifts in bulk alloys and surface adlayers. Phys Rev B 1995;51:17168–80.
[38] Santasalo-Aarnio A, Tuomi S, Jalkanen K, Kontturi K, Kallio T. The correlation of electrochemical and fuel cell results for alcohol oxidation in acidic and alkaline media. Electrochim Acta 2013;87:730–8.
[39] Jiang L, Hsu A, Chu D, Chen R. Ethanol electro-oxidation on Pt/C and PtSn/C catalysts in alkaline and acid solutions. Int J Hydrogen Energy 2010;35:365–72.
[40] Ma L, Chu D, Chen R. Comparison of ethanol electro-oxidation on Pt/C and Pd/C catalysts in alkaline media. Int J Hydrogen Energy 2012;37:11185–94.
[41] Tripković AV, Štrbac S, Popović KD. Effect of temperature on the methanol oxidation at supported Pt and PtRu catalysts in alkaline solution. Electrochem Commun 2003;5:484–90.
[42] dos Santos L, Colmati F, Gonzalez ER. Preparation and characterization of supported Pt–Ru catalysts with a high Ru content. J Power Sources 2006;159:869–77.
[43] Watanabe M, Motoo S. Electrocatalysis by ad-atoms: Part II. Enhancement of the oxidation of methanol on platinum by ruthenium ad-atoms. J Electroanal Chem Interfacial Electrochem 1975;60:267–73.
[44] Sugimoto W, Aoyama K, Kawaguchi T, Murakami Y, Takasu Y. Kinetics of CH_3OH oxidation on PtRu/C studied by impedance and CO stripping voltammetry. J Electroanal Chem 2005;576:215–21.
[45] Kim HJ, Choi SM, Green S, Tompsett GA, Lee SH, Huber GW, et al. Highly active and stable PtRuSn/C catalyst for electrooxidations of ethylene glycol and glycerol. Appl Catal B Environ 2011;101:366–75.
[46] Sieben JM, Duarte MME. Methanol, ethanol and ethylene glycol electro-oxidation at Pt and Pt–Ru catalysts electrodeposited over oxidized carbon nanotubes. Int J Hydrogen Energy 2012;37:9941–7.
[47] Bang JH, Han K, Skrabalak SE, Kim H, Suslick KS. Porous carbon supports prepared by ultrasonic spray pyrolysis for direct methanol fuel cell electrodes. J Phys Chem C 2007;111:10959–64.
[48] Deivaraj TC, Lee JY. Preparation of carbon-supported PtRu nanoparticles for direct methanol fuel cell applications – a comparative study. J Power Sources 2005;142:43–9.
[49] Liu Z, Ling XY, Guo B, Hong L, Lee JY. Pt and PtRu nanoparticles deposited on single-wall carbon nanotubes for methanol electro-oxidation. J Power Sources 2007;167:272–80.
[50] Zhu J, Su Y, Cheng F, Chen J. Improving the performance of PtRu/C catalysts for methanol oxidation by sensitization and activation treatment. J Power Sources 2007;166:331–6.